Università degli Studi di Padova

Departement of Industrial Engineering

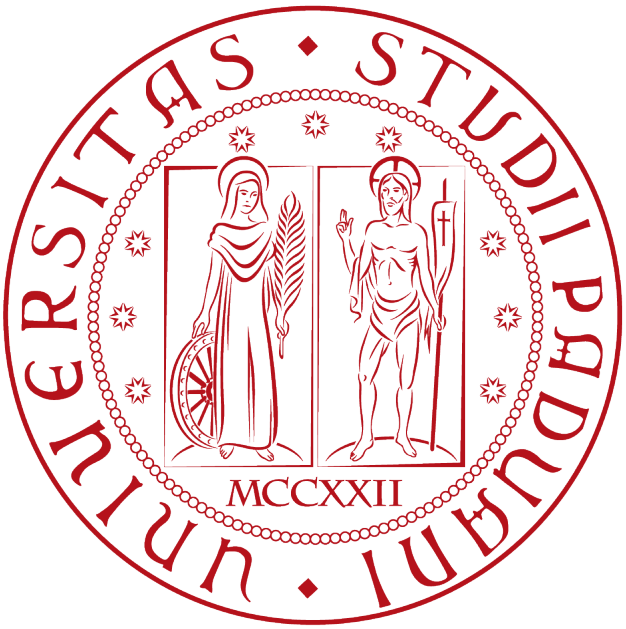

Master Degree in Aerospace Engineering

Numerical Simulation of a 2D Swimming Fish: Analysis of the Tail Beat Frequency's Role

---

Thesis Advisor:

Prof. **Francesco Picano**

Candidate:

Emma Rosa

MATR. 1236489

Thesis Co-advisor:

Dr. **Federico Dalla Barba** PhD

To my family

Abstract

Fish locomotion has attracted the attention of many scientists throughout the centuries and nowadays, with the increasing interest in the environmental issues, it has become an important subject. Thanks to the recent developments of computational fluid dynamics we are able to perform numerical simulations that allow us to explore different aspects of fish motion. With the aid of a 2D numerical model, the present study focuses on the role of the deformation amplitude and the tail beat frequency for three different types of kinematics and for two different Reynolds numbers. An estimation of the efficiency has also been attempted both through the EBT model and with the classical definition of efficiency, although the matter is complicated and needs further investigation. In conclusion, an analysis of the different types of wake formed behind a swimming fish is given.

Sommario

Lo studio del moto dei pesci ha attirato l'attenzione di molti scienziati nel corso dei secoli e al giorno d'oggi, con l'interesse crescente verso le tematiche ambientali, questo argomento acquisisce un'importanza sempre maggiore. Grazie ai recenti sviluppi della fluidodinamica computazionale, è possibile realizzare modelli numerici che permettono di esplorare diversi aspetti relativi al moto dei pesci. Con l'aiuto di un modello numerico 2D, questo studio si concentra sul ruolo dell'ampiezza della deformazione e del battito della coda per tre diversi tipi di cinematica e per due diversi numeri di Reynolds. E' stato inoltre tentato il calcolo dell'efficienza, sia attraverso il modello EBT che attraverso una definizione classica di efficienza, sebbene la questione sia complicata e necessiti di ulteriori approfondimenti. In conclusione sono stati analizzati diversi tipi della scia che si forma al passaggio di un pesce.

Acknowledgements

First of all, I would like to thank Professor Francesco Picano and Doctor Federico Dalla Barba for guiding me through this work and for everything they taught me. I am grateful to my family for all the love and support they gave me, especially to my parents for allowing me to pursue my dreams, and to my sisters because they have always been my role models. Thanks to Gabriele for sharing this journey with me through the good and the bad times, and lastly thanks to Giulia, Sofia, Andrea, Alberto, Marco, Simone, Sara and Giada for being the best friends I could ever wish for.

Contents

1 Introduction **1**

2 Fish kinematics **3**

2.1 A classification of fishes 3

2.2 Fish locomotion 4

2.3 Anguilliform and carangiform swimming 5

2.4 Fish vortex street 6

2.5 Efficiency evaluation 8

3 Numerical model **11**

3.1 Body shape and kinematics 11

3.2 Fluid structure interaction 13

3.3 The code 14

3.4 Nondimensionalization 15

4 Velocity Analysis **17**

4.1 Simulation parameters 17

4.2 First tests: mean velocity analysis 19

4.3 Maximum and minimum velocity 21

4.4 Strouhal number and Reynolds number 22

4.5 Second tests: mean velocity analysis 23

4.6 Maximum and minimum velocity 28

4.7 Strouhal number and Reynolds number 31

4.8 Simulations with varying period 35

4.9 Analysis of the behaviour of the synthetic kinematic 38

5 Efficiency estimation with EBT **41**

6 Power estimation **47**

7 Wake observation **55**

8 Conclusion **57**

Chapter 1

Introduction

It is well known that the greatest scientific discoveries come from the observation and understanding of nature and her mechanisms. In the engineering field, we see various examples, indeed many innovations are inspired by the animal kingdom. Among all, fish swimming has been a scientists' subject of interest for centuries: their locomotion was first studied by Leonardo Da Vinci and two hundred years later by Borrelli, who illustrated the crucial role of the tail in his book "De motu animalium". However, the biggest steps forward were made starting from the end of the 19th century. Thanks to the development of experimental research, zoologists were able to categorize fishes by the shape of their body, tail, fins and appendages. These findings were useful to biologists, engineers and mathematicians, like Gray, who studied the kinematics of aquatic animals and Taylor, who later developed the resistive model. On the other hand, Lighthill and Wu proposed the reactive model and introduced the problem of efficiency and propulsive power.

During the last decades, computational fluid dynamics allowed us to build 2D and 3D models, which helped us investigate other aspects of fish locomotion. For instance, countless studies analysed the vorticity release of the fish and insisted on the energy and forces exchange, while considering different species and styles of swimming.

Nowadays, with the increasing interest in the environmental issues, understanding the behaviour of fish has become particularly relevant, for example when building alternative watercourses for fish, to prevent dams and other man-made water structures from obstructing their way. Using numerical tools, we are interested in having a better understanding of the self-propulsion mechanism of fish and their efficiency, believing that our study could bring an important contribution to any kind of application.

Chapter 2

Fish kinematics

2.1 A classification of fishes

The locomotion of fish depends on the species, the body shape, the shape of the tail and fins, and on the style of swimming, which in turn depends on the kind of "mission" the fish has to accomplish, whether its cruising or a fast maneuver.

Observing the main types of locomotion, we can make a distinction between anguilliform, carangiform, subcarangiform and thunniform.

Eels and lampreys are obviously anguilliform fish *fig:2.1.a*. They have long and narrow bodies, whose width remains constant from head to tail and their caudal fins are rounded or totally absent.

On the other hand, carangiform fish, like mackerels *fig:2.1.b*, have thicker bodies, which become thinner towards the peduncle, where the tail attaches to the body. Their body mass is therefore concentrated in the anterior part of the fish.

Subcarangiform fish are similar to the carangiform ones, but their maneuverability is reduced. Trouts belong to this category.

Finally, thunniform swimmers, like tunas and some types of sharks, are the best at cruising, their propulsion is mainly due to the movements of the peduncle and their large and crescent shaped tail.

Figura 2.1.a

Figura 2.1.b

Our work will concentrate on the anguilliform and carangiform modes, since they are the main swimming styles.

2.2 Fish locomotion

Sir James Gray was the first who described the propulsive mechanism of an eel, as a result of the metachronal waves that pass over the surface of the body. This means that due to the rhythmical muscular activity, each section of the fish moves changing its shape and position, making it appear like a wave of contraction passing through the body.
According to Gray, as the wave of muscular contraction passes along the body of the eel, every part of the fish moves forward along a sinusoidal curve and the surface of the body is inclined backwards at a certain angle to its path of motion. The role of this angle is crucial, since it allows the fish to deflect the water backwards and so propel himself through the water.
Another important aspect is the backward velocity of transmission of the waves. Gray demonstrated that the greater the difference between the forward speed of the fish compared with the backward velocity of transmission of the waves, the larger is the angle between the body and the path of motion, which brings to an increase of propulsive thrust as well as of the expenditure of muscular energy. This conclusion comes from the observation of the plots of the idealised swimming gait of an eel, in which the amplitude of the sinusoidal wave remains constant along the body.
The motion of an eel is explained as follows: when the fish is at rest and a wave passes down its body, the angle of attack is at first of maximum value and the thrust is high. Consequently, the fish gathers speed until the angle of attack gives a thrust that is equal to the resisting force, meanwhile there has been a reduction in the rate at which the muscular waves travel backwards. An acceleration corresponds again to and increase in the angle of attack and so on.

Thanks to the observation of experimental data, Gray also deduced that the speed of propagation of the waves is reduced towards the tail of the eel. This could be linked to the fact that this kind of fish have a less developed musculature in this region. Given the fact that, as said before, the wave velocity and the muscular energy are proportional, these to quantities are strongly correlated: a variation in one implies an alteration in the other.

2.3 Anguilliform and carangiform swimming

The motion described in the previous section concerns eels in particular, but what happens for carangiform fish is quite similar. The mechanism of locomotion is in fact the same: sinusoidal waves of contraction pass along the body of the fish, allowing it to propel itself through the water, but what marks the difference is the amplitude of the curve.

As said before, the style of swimming depends on the shape of the fish. Having a long and narrow body and a small or non-existing tail, anguilliform swimmers undulate most of their body with a wave whose amplitude is large over their entire length (*fig. 2.2*), while their wavelength is usually close to 70% of the body length.

On the other hand, for carangiform swimmers the large-amplitude body undulations are restricted to one-half or one-third of the posterior part of the body, the amplitude increasing sharply in the caudal area (*fig. 2.2*). In this case, the wavelength of their motion is about one body length. [4]

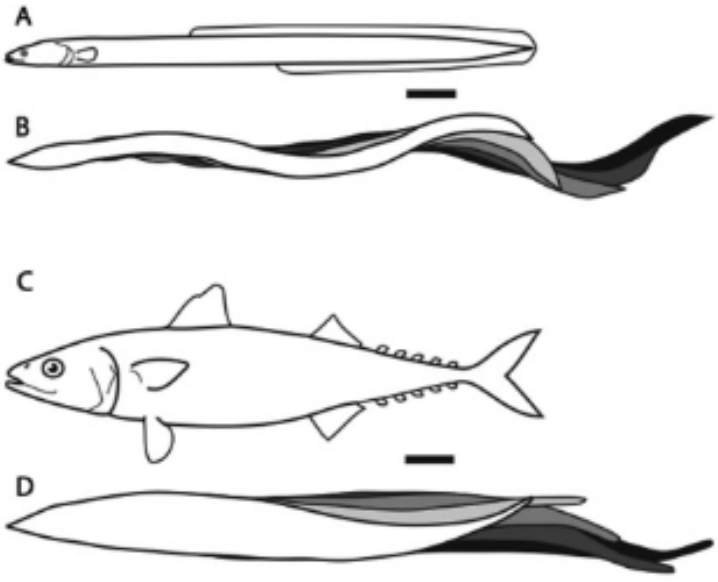

Figure 2.2.: An anguilliform fish (A) and the amplitude variation along its length (B) versus a carangiform fish (C) and the amplitude variation along its length (D)

It is therefore necessary to make a distinction between these two styles of swimming.

2.4 Fish vortex street

When a fish swims, the perturbed water moves and rotates creating a wake called vortex street. These flow structures are also named "fish foot prints", since they bear a lot of information regarding the gait and thrust generation of the fish. [5]

Due to the undulation movement, suction and pressure flows form a circulating flow around the body, which is shed at the tail. Moreover, each time the tail has its maximum lateral displacement and then changes direction, a vortex is shed from the tail tip. More specifically, vortices shed to the left-hand side rotate clockwise, while those shed from the right-hand side rotate counter-clockwise, the two are connected by narrow curved bands of vorticity [7]. Between two consecutive vortices, a jet flow which changes direction with every new vortex being shed, can be seen. [6]

This particular wake structure is called Karman vortex street and it can be regular or inverted, depending on the flapping speed of the tail, and of the direction of the jet between the vortices. If the tail is flapped slowly, we will see a regular Karman vortex street: the vortex dipoles formed by two adjacent fluid vortices will point in the upstream direction, indicating that the open flow has been slowed down by the flapping (*fig.2.3*). However, if the flapping speed increases, which means increasing the tail beat frequency, the dipoles will point downstream creating an inverted Karman vortex street (*fig. 2.4*).

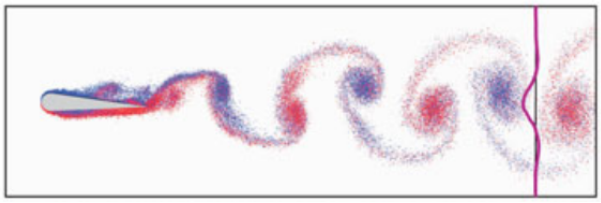

Figure 2.3.: Kàrman vortex street

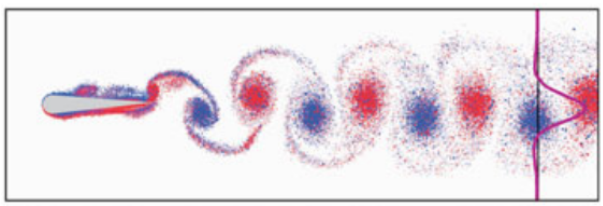

Figure 2.4.: Inverted Kàrman vortex street

According to Muller, the wake morphology is the result of the combination of two vortices: a body-vortex created by the undulatory motion of the body, and a tail-vortex created by the tail beating.

For carangiform fish, the body vortex travels posteriorly along with the body wave and merges with the tail vortex, so that the two vortices are shed together and forming two rows of single counter-rotating vortices, as shown in *fig.2.5* A. For anguilliform fish, however, being devoid of a peduncle region and having a small or non-existent caudal fin, the thrust is mainly produced by the body undulations [8]. For this reason, the body and the tail vortices often do not merge, as shown in *fig.2.5* B. The wake behind an eel can either consist of two rows of single vortices, as seen for the carangiform swimmers, or it can be formed by two rows of double vortices, which means that four vortices per tail-beat cycle are shed, while discrete jets are formed between each vortex pair [4]. The reason of this lies in the phase relationship between the tail beat cycle and the body wave: a phase shift causes the body vortex to be shed offset, instead of on the mean path of motion, which results in the two vortices being separate.

Borazjani and Sotiropoulos found out that the single row occurs at low Strouhal number, while the double row is seen at high Strouhal numbers, the transition from single to double depends on the Reynolds number.

The Strouhal number and Reynold number are defined as:

$$St = \frac{fA}{U} \tag{2.1}$$

$$Re = \frac{Ul}{\nu} \tag{2.2}$$

In the above equations L is the fish length, U is the steady swimming speed, ν is the kinematic viscosity of water, A is the amplitude of the body wave and f is tail-beat frequency. Depending on the direction of the flow between the vortices, the wake can be of drag type or of thrust type. Single vortices wake are usually of drag type for anguilliform fishes, while double vortices patterns are often of thrust type [4].

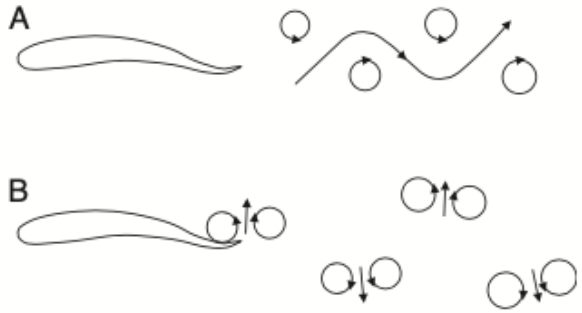

Figure 2.5.: A single vortex wake (A) and a double vortex wake (B)

2.5 Efficiency evaluation

For the eventuality of our study being a starting point for the development of an artificial swimmer, an important aspect is the evaluation of the swimming efficiency, and how it is related to the swimming style and the motion parameters.

Efficiency is defined as the ratio of useful work over expended energy measured over a specific time interval. In our case the useful work is the work needed to overcome the resisting fluid forces, namely the drag, which depends not only on the shape of the body and its speed, but also on the body deformations that are the basis of self-propulsion [9].

Considering a self-propelled flexible body, efficiency is defined as:

$$\eta = \frac{\overline{P_{out}}}{\overline{P_{in}}} \tag{2.3}$$

where P_{in} is the input power and P_{out} is the power output, both these quantities are time-averaged. The latter can be expressed as the product of the net thrust produced by the body (averaged over a period) and its speed.

$$\eta = \frac{\overline{T}U}{\overline{P_{in}}} \tag{2.4}$$

Observing this expression of the efficiency it is clear that this is useful only if the fish is performing a maneuver that requires an acceleration, for example a C-start or an escape maneuver. However, once the fish reaches its cruising speed, the body moves at a constant speed and the total average hydrodynamic forces on the body are equal to zero, therefore equation 2.4 becomes meaningless [9].

The reason of this lies in the difficulties in estimating thrust, since it is strongly connected to the drag, the two quantities cannot be separated [10]. It is therefore necessary to find an

alternative way to express the efficiency of swimming.

To this purpose, Lighthill introduced a model for the estimation of efficiency, called *Elongated body theory* or *EBT*, which is valid under the hypothesis of inviscid flow, two-dimensional simulation, slenderness of the body, small variation in shape and motion, and the angle of the fish tail with the swimming direction should be equal to zero [11].

$$\eta = \frac{1}{2} * (1 + \beta) \tag{2.5}$$

In the above equation $\beta = \mathrm{U/V}$ is the slip ratio, where U is the swimming speed and V is the speed of the backward undulatory body wave, which in turn is defined as the ratio of the pulse ω to the wave number k.

This model provides a good approximation of the efficiency, if separation effects and vorticity shed from body edges are small, and interaction of the body with the shed vorticity is negligeable [9].

In the light of the problems underlined earlier, a more effective way of measuring the efficiency of swimming is by calculating the *Cost of Transportation* or *COT*, which is defined as the ratio of the time-averaged total power needed to swim at a constant velocity, to the swimming speed:

$$COT = \frac{\overline{P_{tot}}}{U} \tag{2.6}$$

The goal is to minimize the value of COT, which means minimizing the energy consumption.

Maertens suggested using the towed resistance instead of the thrust, employing what he calls *quasi-propulsive efficiency*:

$$\eta_{QP} = \frac{RU}{\overline{P_{in}}} \tag{2.7}$$

In the above equation, $\overline{P_{in}}$ is the power required to drive the fish at speed U under steady-state conditions, and R is the towed resistance. This however implies assuming that the fish is still and towed at a constant speed, with the force R compensating the drag, and therefore this expression is not suited for our application.

Chapter 3

Numerical model

3.1 Body shape and kinematics

What we learned from the experimental results of the scientists named in the previous chapters was put into practice through a numerical model. For the sake of simplicity, we decided to carry out our simulations on a 2D numerical model, hoping that the satisfactory results we obtained could be an important starting point for any future development.
The body of the fish at rest is represented by a shape corresponding to a NACA 0012 airfoil with a chord length C equal to 1, and is devoid of any kind of fin or appendage. The lateral displacement h of the mid-line is described by an analytical expression that consists of a travelling wave multiplied by a polynomial amplitude modulation:

$$h(s,t) = A * sin(k * s - \omega * t) \tag{3.1}$$

Where A is the amplitude, k is the wave number defined as the ratio of 2π to the wavelength λ, ω is the angular frequency, t is the time and s is the coordinate along the mid-line.
Moreover, the deformation has been corrected by removing the rigid displacements, in order to maintain the centre of mass' position fixed.
As explained in the previous chapter, different types of fish show a different variation of the amplitude along the body length. In our study, we focused on three types of kinematics, each one having a different analytical expression for the amplitude [14]:

- **Synthetic deformation**: the amplitude has a constant value all along the body length, as shown in *fig. 3.1.* This is an idealised motion, often used in the numerical models and theoretical studies as a simplification.

- **Anguilliform kinematic**: the amplitude increases uniformly towards the tail, as shown in *fig. 3.2* and as described by the following expression:

$$A(s) = 0.1 * e^{(s-1)} \tag{3.2}$$

- **Carangiform kinematic**: the amplitude increases sharply in the tail region, as shown in *fig. 3.3* and as described by the following expression:

$$A(s) = 0.02 - 0.08 * s + 0.16 * s^2 \tag{3.3}$$

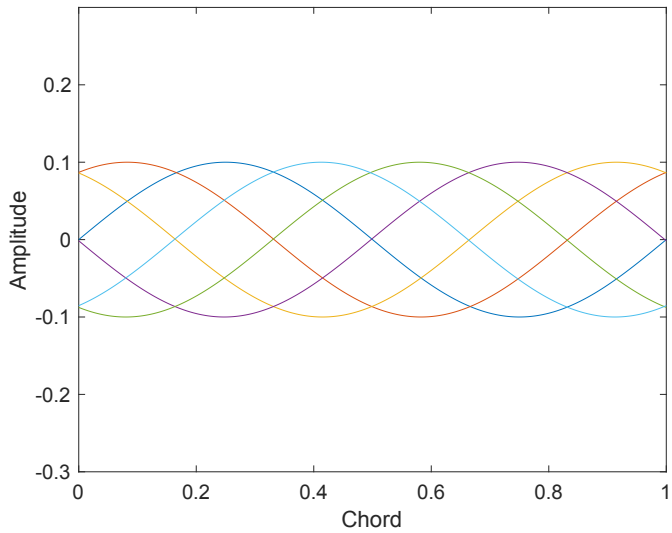

fig. 3.1 Synthetic deformation: amplitude variation along the length of the body

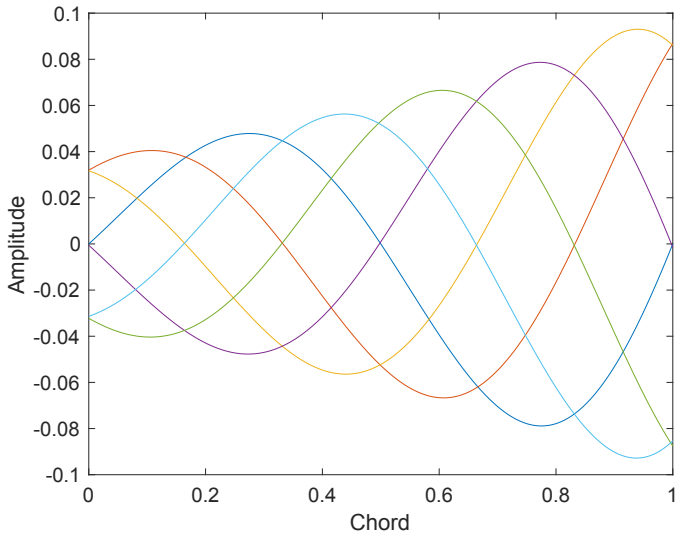

fig. 3.2 Anguilliform kinematic: amplitude variation along the length of the body

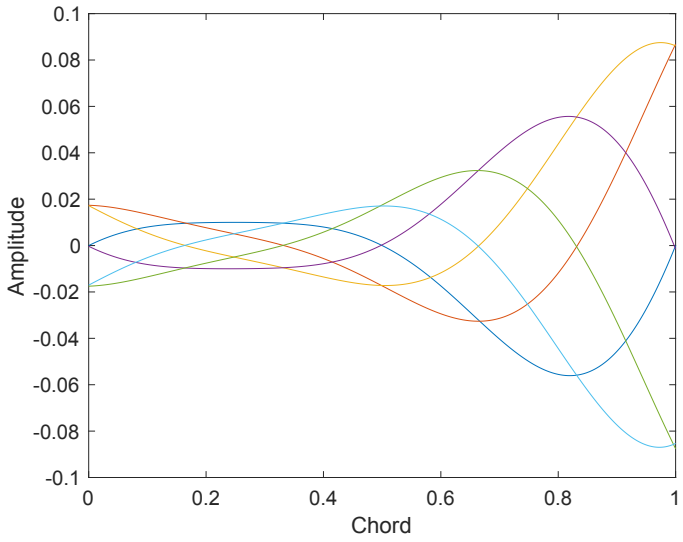

fig. 3.3 Carangiform kinematic: amplitude variation along the length of the body

3.2 Fluid structure interaction

The flow past a swimming fish is a clear example of a *fluid structure interaction problem* or *FSI*, which presents significant challenges to numerical simulations, especially when the boundaries are complex, immersed and deforming like in our case. Based on how the boundaries are treated, numerical algorithms solving FSI problems can be categorized into *conforming mesh methods* and *non-conforming mesh methods*. The first one implies a continuous remeshing to allow the conforming of the mesh to the interface. The second one does not need remeshing, hence it is preferable in our case, since we deal with a deforming body [13].

We applied the *Immersed Boundary Method* or *IBM* to solve the FSI problem, for which the flow fields are strongly influenced by the presence of the fish, a structure with immersed moving boundaries.

The flow is governed by the incompressible Navier-Stokes equations:

$$\begin{cases} \nabla \cdot \mathbf{u} = 0 \\ \rho \left(\frac{\partial \mathbf{u}}{\partial t} + \mathbf{u} \cdot \nabla \mathbf{u} \right) = -\nabla p + \mu \nabla^2 \mathbf{u} + \mathbf{f} \end{cases} \tag{3.4}$$

where $\mathbf{u}$ is the velocity vector, p is the pressure, ρ is the density, μ is the ratio of the kinematic viscosity of water ν to the density, and $\mathbf{f}$ is the force vector that results from the interactions between the solid body and the fluid flow, which is the key element that accounts for the presence of the body.

The IBM consists in applying a fictitious force to the flow in proximity of the interfaces so that the flow is locally forced to move with the same local velocity of the boundary. By doing so, the boundary conditions are not directly imposed, but are however indirectly satisfied [12]. Furthermore, the fish is initially still until it starts undulating with its prescribed motion and therefore it has an acceleration until it reaches a steady velocity. At first, the thrust is generated by the interactions with the flow, then a drag force is produced owing to the viscosity of the fluid. Initially the drag force is smaller than the thrust, therefore the speed increases as well as the drag force, until thrust and drag are balanced and the fish begins moving with a constant average velocity [13]. During this process, the governing equation is Newton's second law:

$$m\frac{\partial^2 x_c}{\partial t^2} = F \tag{3.5}$$

where m is the mass of the fish, x_c is the coordinate of the fish' centre of gravity in the x-direction and F is the force.
Our model also allows the rotations of the fish, which in turn is governed by the following equation:

$$M = I * \dot{\theta} \tag{3.6}$$

where I is the moment of inertia, $\dot{\theta}$ is the angular velocity and M is the torque.

3.3 The code

As concerns the fluid solver, we employed the open source code *CaNS* which was properly modified to account for the interaction with the immersed solid. The code is able to perform direct numerical simulations of flows by solving the incompressible Navier-Stokes equations [equation 3.4]. For these, space discretization is provided by a second order finite difference scheme, together with a third order Runge-Kutta time marching algorithm, while the pressure-velocity coupling is solved through the pressure correction algorithm. The code runs on Fortran 90 and allows a parallelization through the OpenMP library.

3.4 Nondimensionalization

We are dealing with a problem that involves many physical quantities, therefore a nondimensionalisation was performed to reduce the number of parameters and simplify our code.
A vital parameter of our simulations is the Reynolds number, which is defined as:

$$Re_0 = \frac{U_0 * L_0}{\nu} \tag{3.7}$$

where U_0 and L_0 are the reference speed and length respectively, while ν is the kinematic viscosity of water.
Since U_0 and L_0 are both set to be equal to one, the value of Re_0 is simply equal to the inverse of the kinematic viscosity.
Considering the fact that we are employing a two-dimensional model and that we are dealing with limited computational resources, we decided to perform our simulations setting two different values of Re_0: Re_0=1000 and Re_0=4000.
To clarify our results and bring our quantities back to a dimension, we ask the reader to refer to the following situations:

- A 2.5 cm long fish swimming at a speed $U_0 = 0.04$ m/s for the simulations at $Re_0 = 1000$.
- A 10 cm long fish swimming at a speed $U_0 = 0.04$ m/s for the simulations at $Re_0 = 4000$.

Considering the kinematic viscosity of water ν equal to 10^{-6}. The results concerning velocity (U) should then be multiplied by U_0=0.04 m/s.

Chapter 4

Velocity Analysis

4.1 Simulation parameters

By the analysis of the first results we obtained, we realised that our model relies on three key parameters:

- **Nondimensional amplitude**: $\frac{A}{L_0}$;
- **Nondimensional thickness**: $\frac{h}{L_0}$;
- **Reynolds omega**: $Re_\omega = A * \omega * L_0 * Re_0$.

In the above definitions, A is the amplitude of the wave that passes through the fish' body, h is the thickness of the body, ω is the pulse of the undulation, L_0 is the reference length, which is equal to 1, and Re_0 is the Reynolds number we set into the simulation.
This study will focus in particular in the variation of the nondimensional amplitude, which for convenience will from now on be referred to as "amplitude" and indicated by the letter A, and the consequent variation of the tail beat's frequency. We will also analyse the different types of kinematics described in *Chapter 3*.
The thickness of the fish will remain constant, therefore we are going to employ the NACA 0012 airfoil throughout all of our simulations.
To perform our tests, six amplitude values were chosen. As regards the carangiform and the anguilliform kinematics, the amplitude values refer to the maximum lateral displacement, which is located on the tail, while for the synthetic kinematic, the amplitude remains constant along the length of the fish. Consequently, the expressions *3.2* and *3.3* were multiplied by a proper coefficient in order to obtain maximum lateral displacements equal to the amplitude values chosen.

When varying the amplitude value, the pulse has to change too in order to have a constant value of Re_ω. For this reason, for the simulations at Re_0=1000, we hypothesised a period value of P=0.25 for the amplitude value of A=0.10546 and we calculated the corresponding value of Re_ω = 2650.5. The latter was then used to obtain the corresponding pulse value for each of the amplitude values, through which, remembering that P=$2\pi/\omega$, we calculated the period P of the undulation. The same couples of amplitude and period values were then set for the simulations at Re_0=4000.
For clarity's sake, the numerical values are listed in the following chart.

Amplitude	Period
0.04727	0.1121
0.06254	0.1483
0.07739	0.1835
0.091726	0.2174
0.10546	0.25
0.1185	0.2808

Table 4.1: List of the amplitude and period values used in the simulations.

As explained in the previous chapter, the fish is initially still and has an acceleration until it reaches a constant speed in the x-direction. An important aspect of our study is the evaluation of the mean velocity during the steady part of his motion.
An example of the velocity variation along the x-direction is shown in *Figure 4.1*. As regards the velocity in the y-direction, its value oscillates around zero with a constant amplitude, as shown in *Figure 4.2*, and for this reason it will not be relevant in our analysis.
On the x-axis we have the time of the simulation divided by the period.

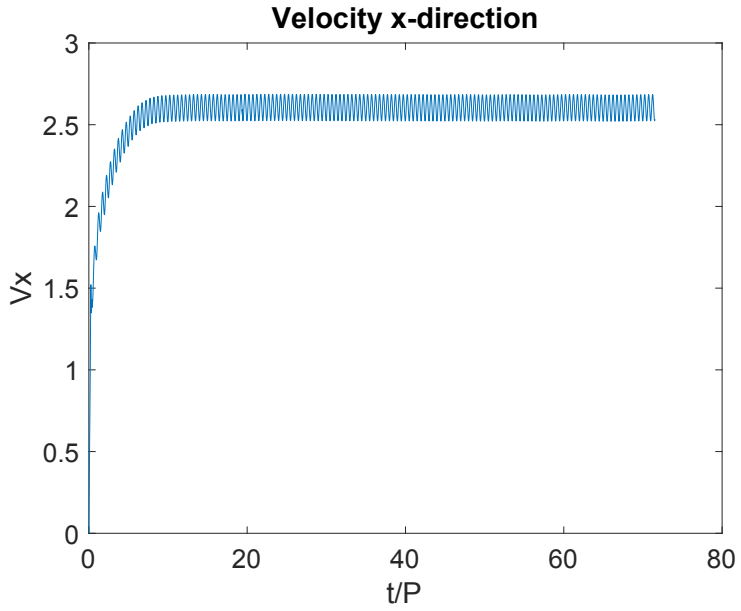

fig. 4.1 Velocity in the x-direction for a fish swimming with the synthetic deformation

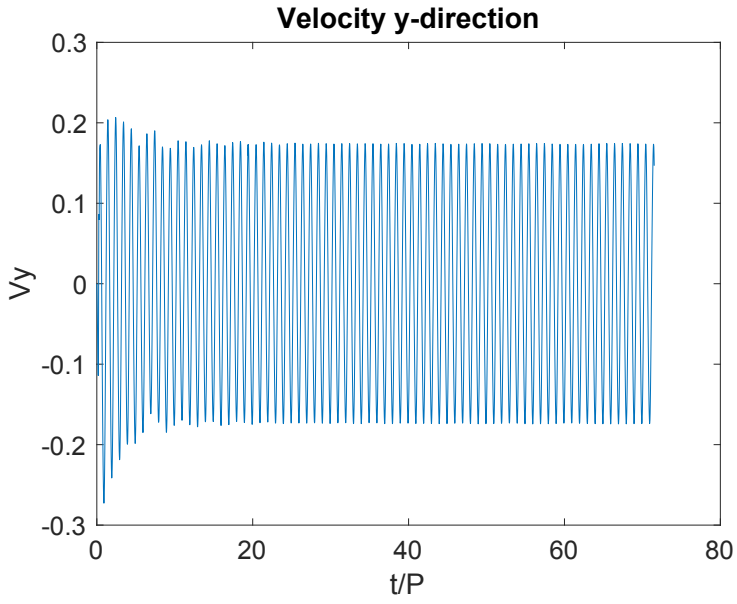

fig. 4.2 Velocity in the y-direction for a fish swimming with the synthetic deformation

4.2 First tests: mean velocity analysis

The first tests were run on a 4x1 rectangular domain and involve the synthetic kinematic, which was tested with three of the selected amplitude values. The number of nodes where:

- 64·4 x 64 for the simulations at $Re_0 = 1000$;
- 64·8 x 64·2 for the simulations at $Re_0 = 4000$.

As regards the boundary conditions of the domains, we set:

- **Uniform inflow** on the left wall;
- **Outflow** on the right wall;
- **Symmetry** on the top and bottom wall;

The velocity results found for both values of Re_0 will be listed in the following chart:

Amplitude	Period	V mean at Re_0=4000	V mean at Re_0=1000	Percentage difference
0.04727	0.1121	4.1534	2.4049	42.09%
0.07739	0.1835	3.0907	2.561	17.13%
0.1185	0.2808	2.2793	1.9587	14.065%

Table 4.2: Mean velocity for the synthetic deformation at Re_0=1000 and at Re_0=4000 and the percentage difference between the two.

By observing these data, we recognize that the mean velocity value increases as the amplitude and the period decrease, or equally, as the amplitude decreases and the frequency increases, and that a higher Re_0 means higher velocity values. At Re_0=1000 however, we notice a different trend: the mean velocity value corresponding to the smallest amplitude is in fact smaller than the velocity value concerning the amplitude of 0.07739. Moreover, the percentage difference for the smaller amplitude is much larger than the other values.
The following plot shows the mean velocity trend:

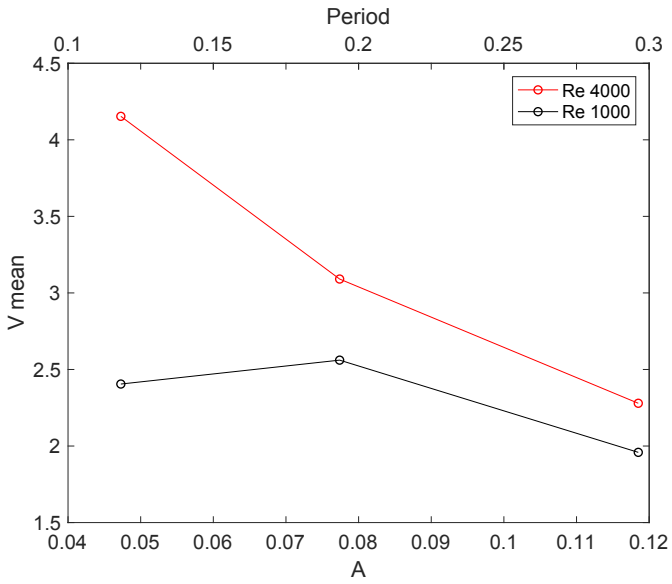

fig. 4.3 Mean velocity synthetic kinematic

4.3 Maximum and minimum velocity

During the steady locomotion, the velocity along the x-direction has oscillations as shown in *Fig.4.1.* We computed the maximum and minimum velocity during the steady trait, together with the difference between the two peaks. Observing the results listed in the following charts, it is clear that the values are quite similar, however, it is not possible to identify a general trend.

Amplitude	Period	V max	V min	Difference
0.04727	0.1121	4.2319	4.0522	0.1797
0.07739	0.1835	3.1818	3.0052	0.1766
0.1185	0.2808	2.3763	2.1304	0.2459

Table 4.3: Synthetic kinematic at Re=4000: maximum and minimum velocity and their difference.

Amplitude	Period	V max	V min	Difference
0.04727	0.1121	2.5038	2.2806	0.2232
0.07739	0.1835	2.6566	2.4261	0.2305
0.1185	0.2808	2.0447	1.8577	0.187

Table 4.4: Synthetic kinematic at Re=1000: maximum and minimum velocity and their difference.

4.4 Strouhal number and Reynolds number

The mean velocity values found in these tests were then used to calculate the Strouhal number and the Reynolds number, with the following expressions:

$$St^* = \frac{f \cdot A}{V_{mean}} \tag{4.1}$$

$$Re^* = V_{mean} \cdot L \cdot Re_0 \tag{4.2}$$

Where f and A are the frequency and the amplitude respectively, L is the length of the fish and Re_0 is the Reynolds number of the simulation. The star indicates that these values are computed with the mean velocity value.

Amplitude	Period	Re^*	St^*
0.04727	0.1121	16613.6	0.1015
0.07739	0.1835	12362.8	0.1365
0.1185	0.2808	9117.2	0.1851

Table 4.5: Synthetic kinematic at Re=4000: Reynolds and Strouhal numbers.

Amplitude	Period	Re^*	St^*
0.04727	0.1121	2404.9	0.1753
0.07739	0.1835	2561	0.1647
0.1185	0.2808	1958.7	0.2155

Table 4.6: Synthetic kinematic at Re=1000: Reynolds and Strouhal numbers.

Being related to the mean velocity, these parameters show a trend that is strictly connected to mean velocity one. More specifically, the Strouhal number trend is the opposite of what found for the velocity: it increases as the amplitude and the period increase, and decreases with Re_0, while the Re^* has the same trend observed for the velocity. What is interesting to notice, is that the Strouhal number value are around 0.2 and 0.1, which agree with the results from previous studies [4].

To make the trend more evident, *Fig. 4.4* shows the Strouhal numbers plot.

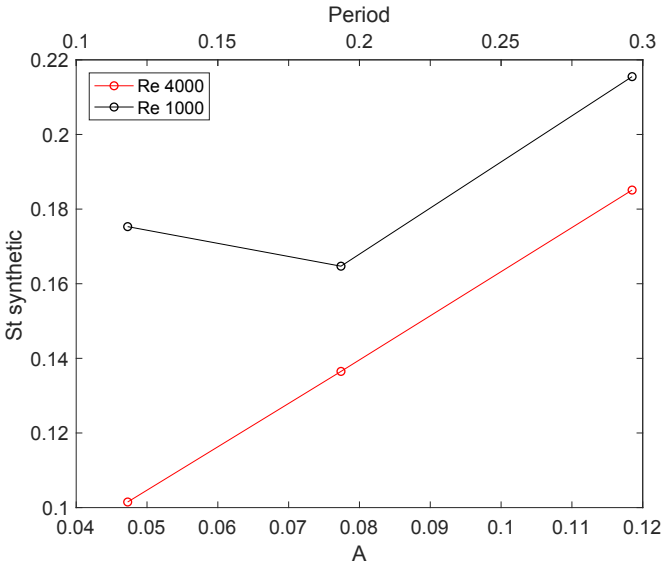

fig. 4.4 Synthetic kinematic: St number.

4.5 Second tests: mean velocity analysis

The tests were performed with all of the amplitude and period values listed in the *Table 4.1* and all of the three swimming styles. The boundary conditions of the domain are the same of the previous simulations, but the following domain sizes and nodes numbers were used:

- Re_0=**4000**: 8x8 domain with 64·8x64·8 nodes;
- Re_0=**1000**: 3x3 domain with 64·3x64·3 nodes.

The mean velocity of the steady fish locomotion was computed and by observing the values that are listed in the following charts, we notice that, the speed increases as the amplitude and the period decrease, and that a higher Re_0 means higher velocity values, as observed in the previous test. As regards the percentage difference of the anguilliform and the carangiform kinematics, it is around 20 and 27 percent. Once again we observe an abnormal behaviour for the synthetic kinematic at Re_0=1000 with the lowest amplitude value. The percentage difference concerning the latter, is still higher than the other values observed. Plots of the mean velocity values against the amplitude for each of the kinematic highlight this behaviour (*Fig. 4.5 Fig. 4.6 and Fig. 4.7*) while the plots at the same Re_0 show that the synthetic kinematic allows the highest velocities, while the anguilliform style is the slowest (*Fig. 4.8 Fig. 4.9*). It is clear that these velocity plots are similar to straight lines, therefore we computed the coefficients of the lines that fit our data (*Tab. 4.10*).

Amplitude	Period	V mean at Re_0=4000	V mean at Re_0=1000	Percentage difference
0.04727	0.1121	3.101	2.4108	22.25%
0.06254	0.1483	2.9396	2.1141	28.08 %
0.07739	0.1835	2.6571	2.0181	24.05%
0.091726	0.2174	2.3879	1.9035	20.285 %
0.10546	0.25	2.2395	1.787	20.205 %
0.1185	0.2808	2.0745	1.6565	20.15%

Table 4.7: Mean velocity for the carangiform kinematic at Re_0=1000 and at Re_0=4000 and the percentage difference between the two.

Amplitude	Period	V mean at Re_0=4000	V mean at Re_0=1000	Percentage difference
0.04727	0.1121	2.6437	2.1449	18.86%
0.06254	0.1483	2.4218	1.8735	22.64 %
0.07739	0.1835	2.2966	1.7221	25.015%
0.091726	0.2174	1.9826	1.586	20 %
0.10546	0.25	1.8225	1.462	19.78 %
0.1185	0.2808	1.7106	1.3479	21.21%

Table 4.8: Mean velocity for the anguilliform kinematic at Re_0=1000 and at Re_0=4000 and the percentage difference between the two.

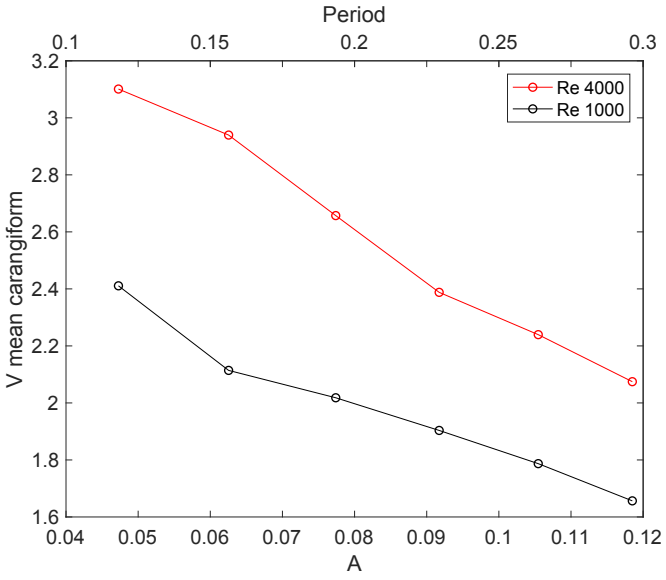

fig. 4.5 Carangiform kinematic mean velocity.

Amplitude	Period	V mean at Re_0=4000	V mean at Re_0=1000	Percentage difference
0.04727	0.1121	3.7261	2.3529	36.85%
0.06254	0.1483	3.4736	2.8519	17.9 %
0.07739	0.1835	3.1583	2.6065	17.47%
0.091726	0.2174	2.8997	2.3756	18.07 %
0.10546	0.25	2.6598	2.1893	17.7 %
0.1185	0.2808	2.2147	2.0608	6.94%

Table 4.9: Mean velocity for the synthetic kinematic at Re_0=1000 and at Re_0=4000 and the percentage difference between the two.

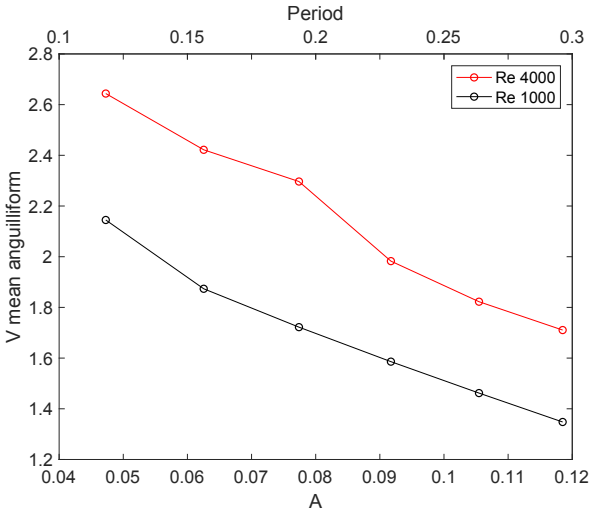

fig. 4.6 Anguilliform kinematic mean velocity.

Kinematic	Re_0	m	q
Carangiform	4000	-15.0346	3.8275
Carangiform	1000	-9.778	2.8012
Anguilliform	4000	-13.5876	3.2851
Synthetic	4000	-20.4916	4.7395
Synthetic	1000	-7.2226	3.0115

Table 4.10: Coefficients of the lines that fit the mean velocity data

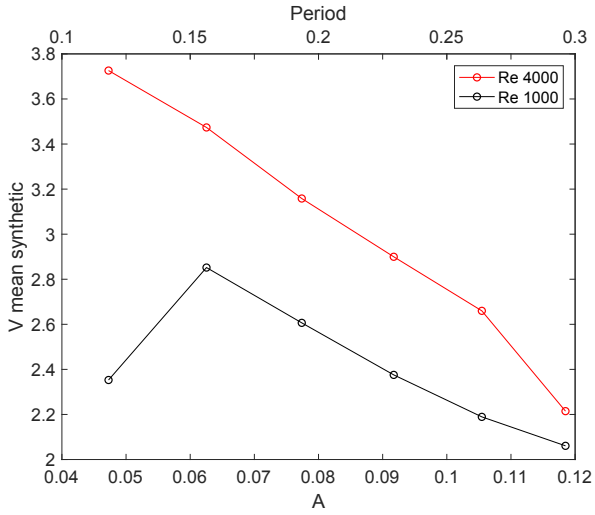

fig. 4.7 Synthetic kinematic mean velocity.

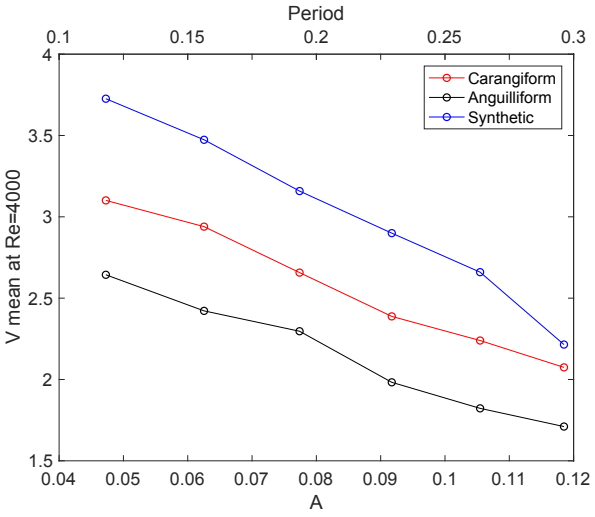

fig. 4.8 Mean velocity at Re=4000.

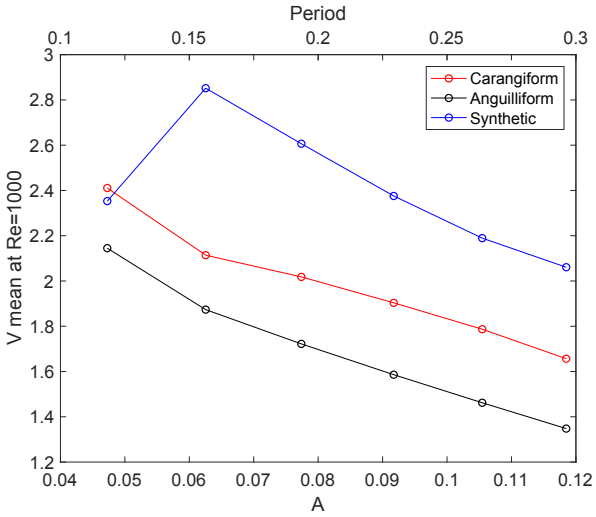

fig. 4.9 Mean velocity at Re=1000.

4.6 Maximum and minimum velocity

We computed the maximum and minimum peaks on the steady part of the motion (*Tab. 4.11, Tab. 4.12, Tab. 4.13, Tab. 4.14, Tab. 4.15 and Tab. 4.16*). As observed during the first tests, the difference between the maximum and minimum values are quite similar, but we notice slightly higher values for the synthetic kinematic. However, it would be impossible to find a general trend, since the results are varied.

Amplitude	Period	V max	V min	Difference
0.04727	0.1121	3.1321	3.0624	0.0697
0.06254	0.1483	2.9608	2.9161	0.0447
0.07739	0.1835	2.6824	2.624	0.0584
0.091726	0.2174	2.4093	2.367	0.0423
0.10546	0.25	2.27	2.2071	0.0629
0.1185	0.2808	2.1025	2.0409	0.0616

Table 4.11: Carangiform kinematic at Re=4000: maximum and minimum velocity

Amplitude	Period	V max	V min	Difference
0.04727	0.1121	2.4449	2.3741	0.0708
0.06254	0.1483	2.1448	2.0846	0.0602
0.07739	0.1835	2.0532	1.9774	0.0758
0.091726	0.2174	1.93	1.869	0.061
0.10546	0.25	1.8187	1.7438	0.0749
0.1185	0.2808	1.6979	1.6179	0.08

Table 4.12: Carangiform kinematic at Re=1000: maximum and minimum velocity

Amplitude	Period	V max	V min	Difference
0.04727	0.1121	2.6666	2.622	0.0446
0.06254	0.1483	2.4591	2.3903	0.0688
0.07739	0.1835	2.3095	2.2817	0.0278
0.091726	0.2174	1.9982	1.9665	0.0317
0.10546	0.25	1.842	1.7975	0.0445
0.1185	0.2808	1.7287	1.6879	0.0408

Table 4.13: Anguilliform kinematic at Re=4000: maximum and minimum velocity

Amplitude	Period	V max	V min	Difference
0.04727	0.1121	2.2475	2.0258	0.2217
0.06254	0.1483	1.8901	1.8495	0.0406
0.07739	0.1835	1.7455	1.6948	0.0507
0.091726	0.2174	1.6243	1.5528	0.0715
0.10546	0.25	1.4904	1.4394	0.051
0.1185	0.2808	1.3723	1.3292	0.0431

Table 4.14: Anguilliform kinematic at Re=1000: maximum and minimum velocity

Amplitude	Period	V max	V min	Difference
0.04727	0.1121	3.8095	3.6368	0.1727
0.06254	0.1483	3.571	3.3715	0.1995
0.07739	0.1835	3.2854	3.0336	0.2518
0.091726	0.2174	3.0129	2.7836	0.2293
0.10546	0.25	2.7809	2.5053	0.2753
0.1185	0.2808	2.2984	2.1399	0.1585

Table 4.15: Synthetic kinematic at Re=4000: maximum and minimum velocity

Amplitude	Period	V max	V min	Difference
0.04727	0.1121	2.4479	2.2599	0.188
0.06254	0.1483	2.9291	2.768	0.1611
0.07739	0.1835	2.6869	2.5207	0.1662
0.091726	0.2174	2.4569	2.2903	0.1666
0.10546	0.25	2.2745	2.1034	0.1711
0.1185	0.2808	2.1348	1.9755	0.1593

Table 4.16: Synthetic kinematic at Re=1000: maximum and minimum velocity

4.7 Strouhal number and Reynolds number

Through the mean velocity values we computed the Strouhal and Reynolds number, whose expressions are *4.1* and *4.2*. Being proportional to the mean velocity, the Reynolds number has the same trend of the velocity, while the Strouhal number has the opposite as shown in (*Fig. 4.10, Fig. 4.11, Fig. 4.12, Fig. 4.13 and Fig. 4.14*). The Strouhal numbers, which are listed at *Tab. 4.17, Tab. 4.18, Tab. 4.19, Tab. 4.20, Tab. 4.21 and Tab. 4.22*, are around 0.2 with a maximum of 0.3131 and a minimum of 0.1132, which again agrees with previous studies.

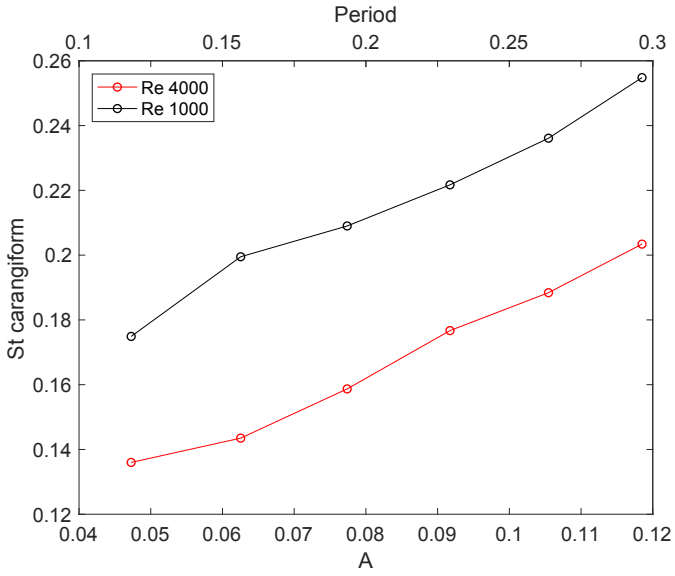

fig. 4.10 Carangiform kinematic: St number.

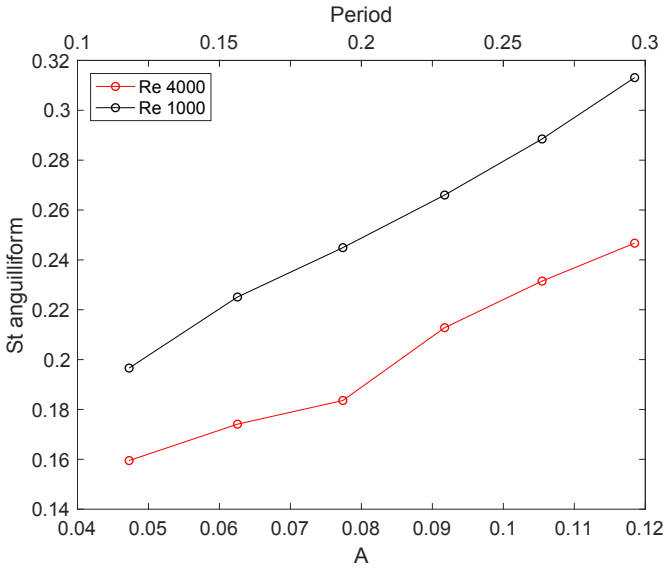

fig. 4.11 Anguilliform kinematic: St number.

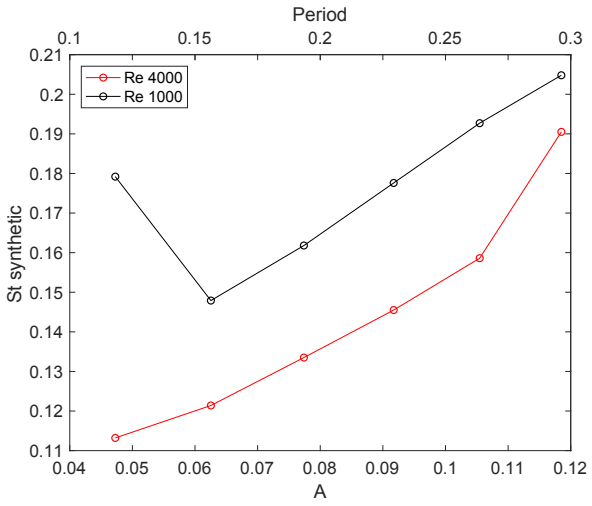

fig. 4.12 Synthetic kinematic: St number.

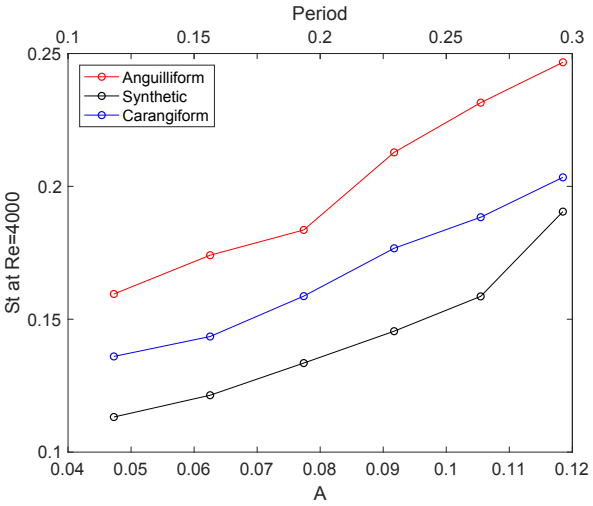

fig. 4.13 St number at Re=4000.

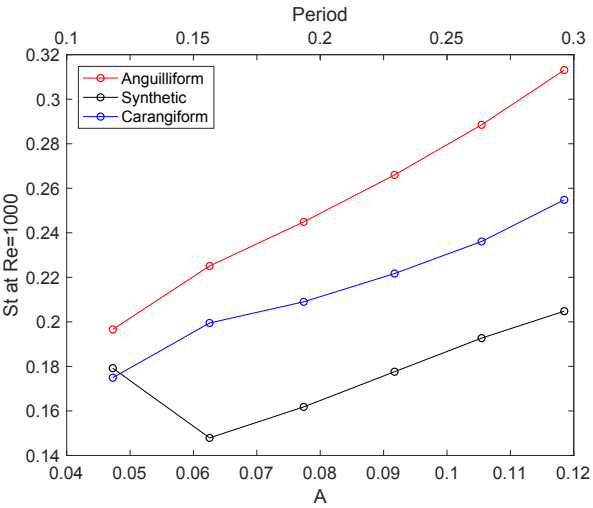

fig. 4.14 St number at Re=1000.

Amplitude	Period	Re^*	St^*
0.04727	0.1121	12404	0.136
0.06254	0.1483	11758.4	0.1435
0.07739	0.1835	10628.4	0.1587
0.091726	0.2174	9551.6	0.1767
0.10546	0.25	8958	0.1884
0.1185	0.2808	8298	0.2034

Table 4.17: Carangiform kinematic at Re=4000 Strouhal and Reynolds number.

Amplitude	Period	Re^*	St^*
0.04727	0.1121	2410.8	0.1749
0.06254	0.1483	2114.1	0.1995
0.07739	0.1835	2018.1	0.209
0.091726	0.2174	1903.5	0.2217
0.10546	0.25	1787	0.2361
0.1185	0.2808	1656.5	0.2548

Table 4.18: Carangiform kinematic at Re=1000 Strouhal and Reynolds number.

Amplitude	Period	Re^*	St^*
0.04727	0.1121	10574.8	0.1595
0.06254	0.1483	9687.2	0.1741
0.07739	0.1835	9186.4	0.1836
0.091726	0.2174	7930.4	0.2128
0.10546	0.25	7290	0.2315
0.1185	0.2808	6842.4	0.2467

Table 4.19: Anguilliform kinematic at Re=4000 Strouhal and Reynolds number.

Amplitude	Period	Re^*	St^*
0.04727	0.1121	2144.9	0.1966
0.06254	0.1483	1873.5	0.2251
0.07739	0.1835	1722.1	0.2449
0.091726	0.2174	1586	0.266
0.10546	0.25	1462	0.2885
0.1185	0.2808	1347.9	0.3131

Table 4.20: Anguilliform kinematic at Re=1000 Strouhal and Reynolds number.

Amplitude	Period	Re^*	St^*
0.04727	0.1121	14904.4	0.1132
0.06254	0.1483	13894.4	0.1214
0.07739	0.1835	12633.2	0.1335
0.091726	0.2174	11598.8	0.1455
0.10546	0.25	10639.2	0.1586
0.1185	0.2808	8858.8	0.1905

Table 4.21: Synthetic kinematic at Re=4000 Strouhal and Reynolds number.

Amplitude	Period	Re^*	St^*
0.04727	0.1121	2352.9	0.1792
0.06254	0.1483	2851.9	0.1479
0.07739	0.1835	2606.5	0.1618
0.091726	0.2174	2375.6	0.1776
0.10546	0.25	2189.3	0.1927
0.1185	0.2808	2060.8	0.2048

Table 4.22: Synthetic kinematic at Re=1000 Strouhal and Reynolds number.

4.8 Simulations with varying period

The aim of this study is understanding how the fish gait changes with the tail beat frequency and the amplitude of the deformation, therefore, in addition to the previous tests we performed a set of simulations with constant amplitude and varying period. The tests were carried out with the synthetic kinematic and with the following domains and nodes number:

- Re_0=**1000**: 3x3 domain with 64·3x64·3 nodes;
- Re_0=**4000**: 8x8 domain with 64·8x64·8 nodes.

and the following boundary conditions on the domain:

- **Uniform inflow**: on the left wall;
- **Outflow**: on the right wall;
- **Symmetry**: on the top and bottom walls.

We tested two amplitude values: A=0.06 and A=0.11, for both of which we performed three simulations for every Re_0 value, setting the following period values:

- Re_0=**1000**:
  - P=0.1;
  - P=0.15;
  - P=0.2.
- Re_0=**4000**:
  - P=0.4;
  - P=0.6;
  - P=0.8.

The mean velocity values are listed in *Tab. 4.23 and Tab. 4.24.*

These results are particularly interesting since they show the velocity trend both with a constant period and varying amplitude, and with a constant amplitude and a varying period. Observing the *Fig. 4.15 and Fig. 4.16* it is clear that swimming with a constant deformation amplitude and an increasing period value, or equally with a decreasing frequency value, leads

Period	V mean for A=0.06	V mean for A=0.11	Percentage difference
0.4	1.0961	1.5319	28.44 %
0.6	0.6617	0.9928	33.35 %
0.8	0.4276	0.7329	41.65 %

Table 4.23: Synthetic kinematic at Re=4000 mean velocity at A=0.06 and at A=0.11 and their percentage difference.

Period	V mean for A=0.06	V mean for A=0.11	Percentage difference
0.1	4.2138	5.9726	29.44 %
0.15	2.6709	3.9356	32.13 %
0.2	1.7405	2.8652	39.25 %

Table 4.24: Synthetic kinematic at Re=1000 mean velocity at A=0.06 and at A=0.11 and their percentage difference.

to a decreasing mean velocity, while maintaining a constant period and and increasing the amplitude leads to an increase of the mean velocity. This last result is particularly encouraging, since it agrees with what noticed in previous studies [1].

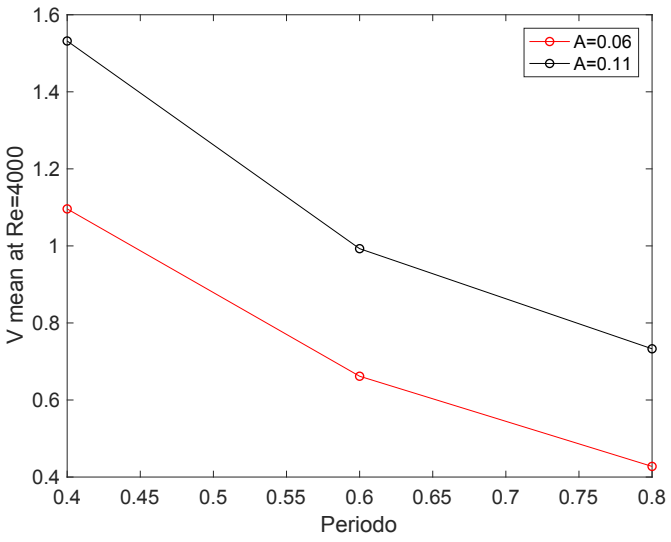

fig. 4.15 Synthetic kinematic: mean velocity at Re=4000.

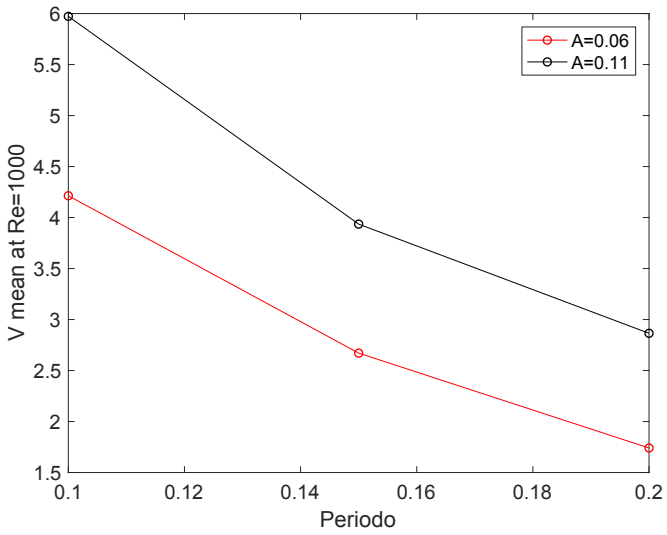

fig. 4.16 Synthetic kinematic: mean velocity at Re=1000.

It is also noticeable that with a higher Re_0 the velocity values decrease, which appears in contrast with what observed in the previous tests. The reason of this behaviour is that the period values for the simulations at Re_0=4000 are higher than the period values for the simulations at Re_0=1000. Repeating the simulations at Re_0=1000 with the same period values as those at Re_0=4000, showed the same trend noticed in the previous tests, since the velocity values for Re_0=1000 become smaller than the ones at Re_0=4000.

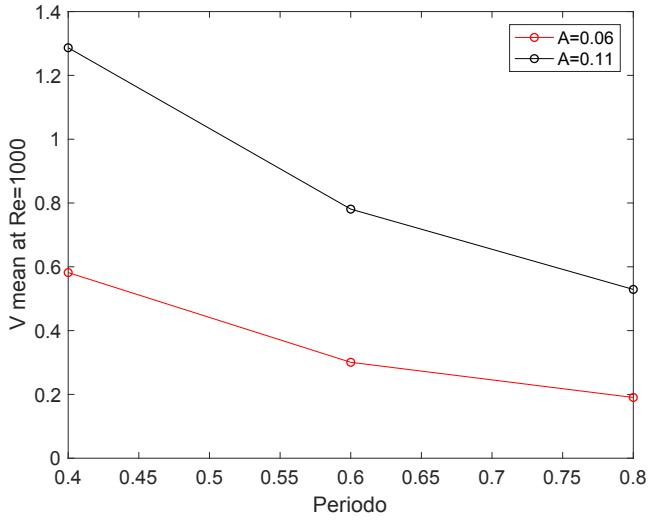

fig. 4.17 Synthetic kinematic: mean velocity at Re=1000, with the same period values as the simulation at Re=4000.

4.9 Analysis of the behaviour of the synthetic kinematic

The results analyzed until now show clearly that the mean velocity and the amplitude are inversely proportional, while the mean velocity and the frequency are directly proportional, nevertheless we noticed an inversion of the trend for the synthetic deformation at Re_0=1000. Further tests were carried out to investigate this abnormal behaviour. We kept the same domain and grid as the first tests, as well as the same boundary conditions on the domain. The amplitude an period values are summarized in the following chart, together with the mean velocity results:

Amplitude	Period	V mean
0.03	0.071	2.0627
0.04727	0.1121	2.4049
0.05	0.1185	2.6614
0.51	0.1208	2.762
0.052	0.123	2.8094
0.053	0.125	2.8954
0.054	0.128	2.9025
0.06254	0.1483	2.849
0.07739	0.1835	2.561
0.1185	0.2808	1.6554

Table 4.25: Synthetic kinematic at Re=1000 mean velocity

We intensified the simulations in the span between the amplitude values 0.04727 and 0.06254, and we notice that the trend has its inversion around the 0.053 amplitude value. as highlighted by the plot at *Fig. 4.18*

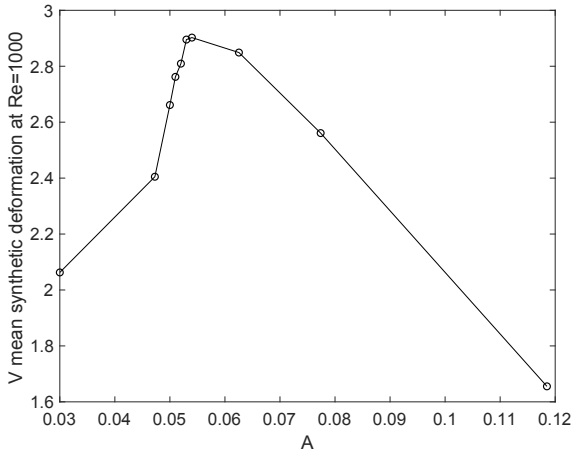

fig. 4.18 Synthetic kinematic: mean velocity at Re=1000

By performing the same simulations using a finer grid however, we recognize the same trend we noticed for the other kinematics, which means that the observed abnormality was due to numerical reasons. *Fig. 4.19* shows the results obtained with a 64·8x64·2 grid on a 4x1 domain.

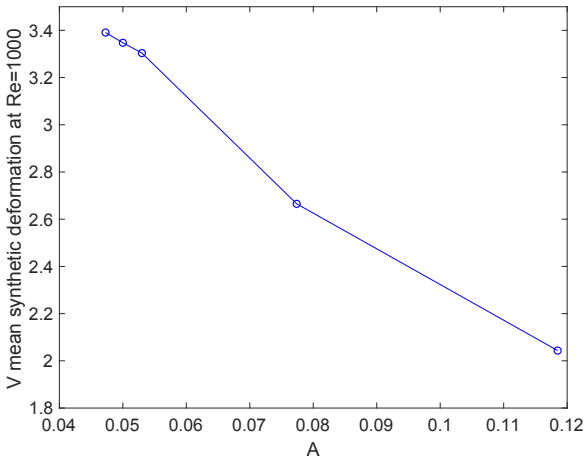

fig. 4.19 Synthetic kinematic: mean velocity at Re=1000 with a finer grid

Chapter 5

Efficiency estimation with EBT

The calculation of the fish swimming's efficiency is an important aspect of our investigation, however, as explained in *Chapter 2*, the matter is complicated. The classical definition of efficiency, whose expression is *Eq. 2.3*, would be meaningless in our case, since we focus on the steady locomotion of the fish, therefore we used the EBT model to find an estimation.
We remind the reader that η_{EBT} is expressed as:

$$\eta_{EBT} = \frac{1}{2} \cdot (1 + \beta) \tag{5.1}$$

Being β=U/V where U is the mean velocity, V=ω/k is the speed of the body wave and remembering that k=$2\pi/\lambda$ and that the pulse ω=2π/P, the above expression becomes:

$$\eta_{EBT} = \frac{1}{2} \cdot (1 + \frac{V_{mean} * P}{\lambda}) \tag{5.2}$$

As explained in *Chapter 2*, the wavelength λ is different for each of the swimming styles, more specifically:

- **Synthetic kinematic:** λ=1;
- **Carangiform kinematic:** λ=0.95;
- **Anguilliform kinematic:** λ=0.642.

The results we obtained are listed in *Tab. 5.1, Tab. 5.2 and Tab. 5.3* and refer to the second tests we performed: *Chapter 4, section 5.*

Amplitude	Period	η_{EBT} at Re_0=4000	η_{EBT} at Re_0=1000
0.04727	0.1121	0.683	0.6422
0.06254	0.1483	0.7294	0.665
0.07739	0.1835	0.7566	0.6949
0.091726	0.2174	0.7732	0.7178
0.10546	0.25	0.7947	0.7351
0.1185	0.2808	0.8066	0.7448

Table 5.1: η_{EBT} for the carangiform kinematic at Re_0=1000 and at Re_0=4000.

Amplitude	Period	η_{EBT} at Re_0=4000	η_{EBT} at Re_0=1000
0.04727	0.1121	0.7308	0.6873
0.06254	0.1483	0.7797	0.7164
0.07739	0.1835	0.8282	0.7461
0.091726	0.2174	0.8357	0.7685
0.10546	0.25	0.8548	0.7847
0.1185	0.2808	0.8741	0.7948

Table 5.2: η_{EBT} for the anguilliform kinematic at Re_0=1000 and at Re_0=4000.

Amplitude	Period	η_{EBT} at Re_0=4000	η_{EBT} at Re_0=1000
0.04727	0.1121	0.7088	0.6319
0.06254	0.1483	0.7576	0.7115
0.07739	0.1835	0.7898	0.7391
0.091726	0.2174	0.8152	0.7582
0.10546	0.25	0.8325	0.7737
0.1185	0.2808	0.8109	0.7893

Table 5.3: η_{EBT} for the synthetic kinematic at Re_0=1000 and at Re_0=4000.

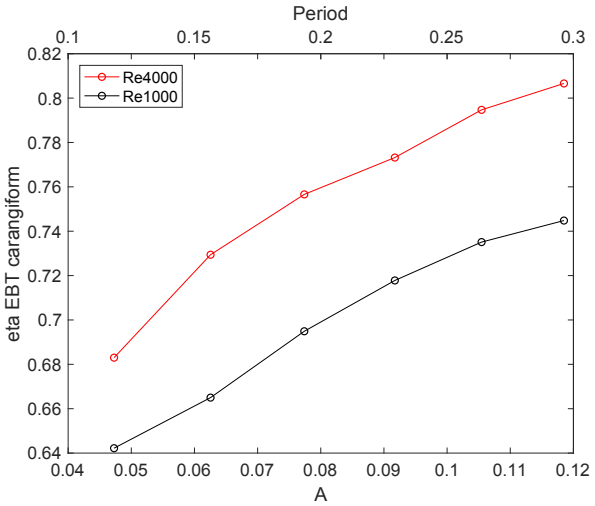

fig. 5.1 Carangiform kinematic: η_{EBT}

By observing *Fig. 5.1, Fig. 5.2 and Fig. 5.3*, we notice that the efficiency increases as the amplitude and the period increase, or as the amplitude increases and the frequency decreases, and that a higher Re_0 means a higher efficiency. From *Fig. 5.4 and Fig. 5.5* we deduce that at the same Re_0 value, the anguilliform kinematic is the most efficient, while the carangiform kinematic is the least efficient.

Remembering the velocity trends we saw in the previous chapter, we can draw the conclusion that under the same Re_0, the higher the speed, the lower the efficiency, and that the anguilliform style of swimming, although being the slowest, ensures the best performance in terms of efficiency.

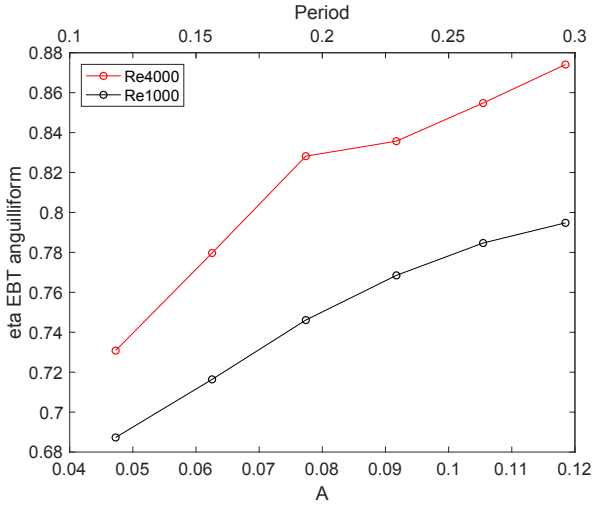

fig. 5.2 Anguilliform kinematic: η_{EBT}

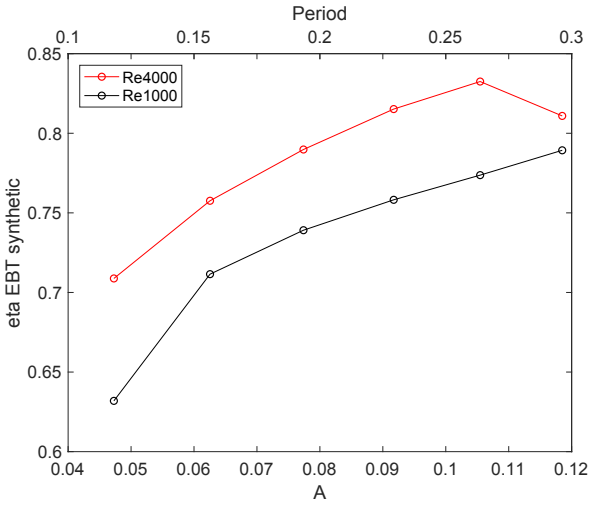

fig. 5.3 Synthetic kinematic: η_{EBT}

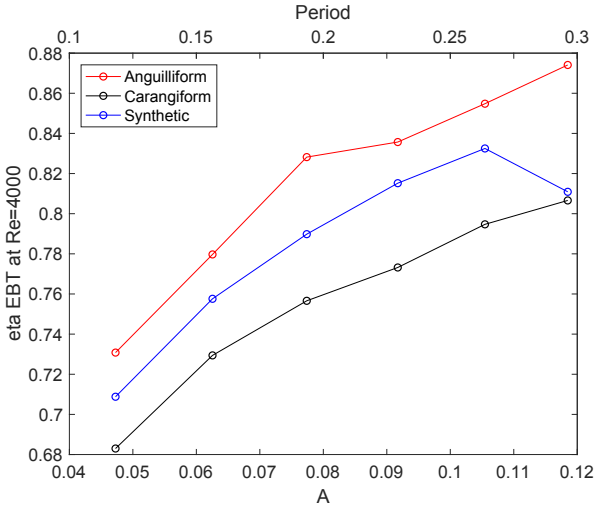

fig. 5.4 η_{EBT} at Re=4000

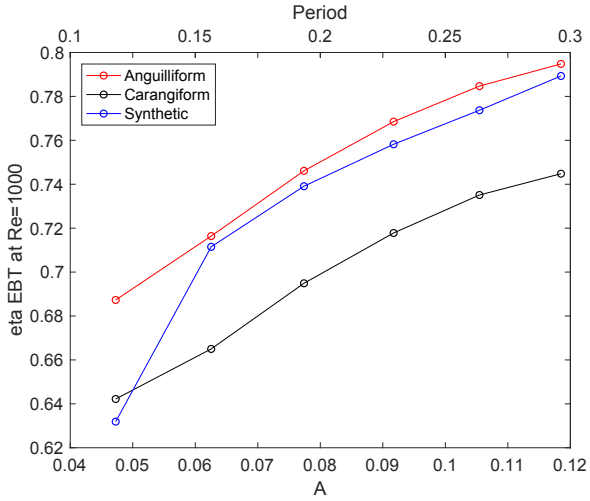

fig. 5.5 η_{EBT} at Re=1000

The results we obtained agree with what observed in previous studies [4], nevertheless, we should keep in mind the fact that this model is not completely suited to our case, since it gives an accurate estimation of the efficiency, only if certain conditions are observed.

Chapter 6

Power estimation

Another interesting aspect of fish locomotion is the power requirement, since it allows to compute parameters that are a measure of the performance of the fish.
The power required for fish locomotion is equal to the sum of the power needed by the fish to maintain a constant velocity during its steady motion, and the power necessary for the deformation. In our code, the power P_{tot} has been obtained by calculating by the following integral:

$$P_{tot} = \oint_S (v_x \cdot \tau_x + v_y \cdot \tau_y)\, ds \tag{6.1}$$

Where τ is the tension and v_x and v_y are the velocity components along the fish outline. The total power has a mean value which is equal to zero, and it is the results of two components: P^+ and P^- which are respectively the power given and absorbed by the flow.
We performed a set of simulations involving all of the three kinematics and three of the amplitude values listed in the *Tab. 4.1.* As regards the boundary conditions of the domain, they were the same as the ones used in the previous tests, while as concerns the domain and grid sizes, the following were employed:

- **Simulations at** Re_0**=4000**: 4x3 domain, 64·8x64·6 nodes;

- **Simulations at** Re_0**=1000**: 3x3 domain, 64·3x64·3 nodes.

The same simulations were then repeated making sure that the fish swam at a constant velocity but without deforming. In doing so, we obtained the power necessary to maintain a certain velocity. The mean velocity and the power components are listed in the *Tab. 6.1, 6.2, 6.3, 6.4, 6.5, 6.6.* Using the power values we obtained, it is possible to compute the efficiency

with the classical definition:

$$\eta = \frac{P_{still}}{P^-} \tag{6.2}$$

P_{still} is in fact the power needed to sustain a certain speed, which is actually the useful power, while P^- is the total power expended for propulsion. The results are listed in *Tab. 6.7 Tab. 6.8 and Tab. 6.9*

Amplitude	Period	V mean	P+	P-	P_{still}
0.04727	0.1121	3.1691	0.0141	0.0213	0.0039
0.07739	0.1835	2.6965	0.0072	0.0122	0.0026
0.1185	0.2808	2.0844	0.004	0.0071	0.0014

Table 6.1: Carangiform kinematic at Re=4000: mean velocity, positive component of the power, absolute value of the negative component of the power and power obtained from the simulation with a still fish, for each of the tested amplitude values.

Amplitude	Period	V mean	P+	P-	P_{still}
0.04727	0.1121	2.4062	0.0397	0.0491	0.0078
0.07739	0.1835	2.0097	0.0183	0.0273	0.0051
0.1185	0.2808	1.6648	0.009	0.0158	0.0032

Table 6.2: Carangiform kinematic at Re=1000: mean velocity, positive component of the power, absolute value of the negative component of the power and power obtained from the simulation with a still fish, for each of the tested amplitude values.

Amplitude	Period	V mean	P+	P-	P_{still}
0.04727	0.1121	2.7586	0.03	0.0338	0.0028
0.07739	0.1835	2.282	0.0152	0.0175	0.0018
0.1185	0.2808	1.6826	0.0086	0.0098	0.000836

Table 6.3: Anguilliform kinematic at Re=4000: mean velocity, positive component of the power, absolute value of the negative component of the power and power obtained from the simulation with a still fish, for each of the tested amplitude values.

Amplitude	Period	V mean	P+	P-	P_{still}
0.04727	0.1121	2.21	0.0896	0.0952	0.0064
0.07739	0.1835	1.6963	0.0433	0.0488	0.0034
0.1185	0.2808	1.3515	0.0265	0.0292	0.002

Table 6.4: Anguilliform kinematic at Re=1000: mean velocity, positive component of the power, absolute value of the negative component of the power and power obtained from the simulation with a still fish, for each of the tested amplitude values.

Amplitude	Period	V mean	P+	P-	P_{still}
0.04727	0.1121	4.1881	0.1019	0.1195	0.0079
0.07739	0.1835	3.2107	0.0557	0.061	0.0041
0.1185	0.2808	2.3404	0.032	0.0348	0.0019

Table 6.5: Synthetic kinematic at Re=4000: mean velocity, positive component of the power, absolute value of the negative component of the power and power obtained from the simulation with a still fish, for each of the tested amplitude values.

Amplitude	Period	V mean	P+	P-	P_{still}
0.04727	0.1121	2.3597	0.2919	0.3113	0.0075
0.07739	0.1835	2.6136	0.1396	0.1537	0.0095
0.1185	0.2808	2.0604	0.0779	0.085	0.0054

Table 6.6: Synthetic kinematic at Re=1000: mean velocity, positive component of the power, absolute value of the negative component of the power and power obtained from the simulation with a still fish, for each of the tested amplitude values.

Amplitude	Period	η at Re=4000	η at Re=1000
0.04727	0.1121	0.1831	0.1589
0.07739	0.1835	0.2131	0.1868
0.1185	0.2808	0.1972	0.2025

Table 6.7: Carangifrom kinematic: efficiency at Re=4000 and Re=1000 for each of the tested amplitude values

Amplitude	Period	η at Re=4000	η at Re=1000
0.04727	0.1121	0.0828	0.0672
0.07739	0.1835	0.1029	0.0697
0.1185	0.2808	0.0853	0.0685

Table 6.8: Anguillifrom kinematic: efficiency at Re=4000 and Re=1000 for each of the tested amplitude values

Amplitude	Period	η at Re=4000	η at Re=1000
0.04727	0.1121	0.0661	0.0241
0.07739	0.1835	0.0672	0.0618
0.1185	0.2808	0.0546	0.0635

Table 6.9: Synthetic kinematic: efficiency at Re=4000 and Re=1000 for each of the tested amplitude values

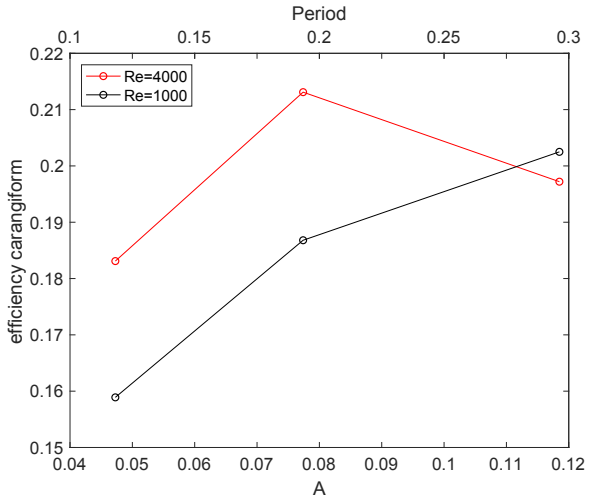

fig. 6.1 Carangiform kinematic: η

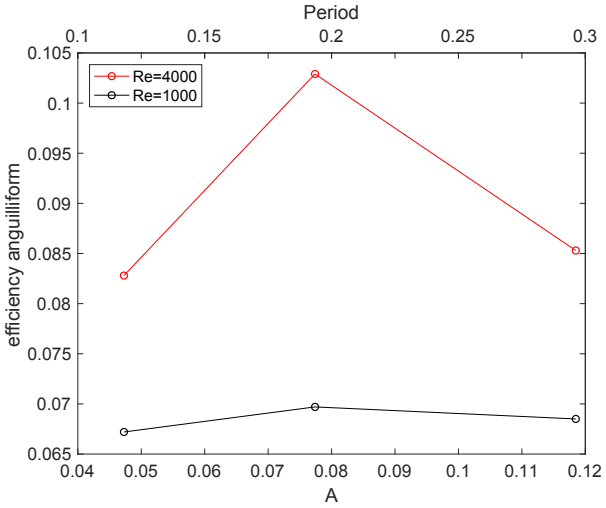

fig. 6.2 Anguilliform kinematic: η

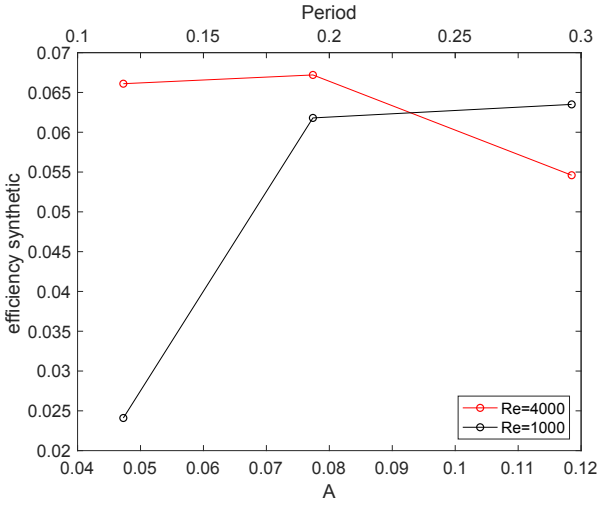

fig. 6.3 Synthetic kinematic: η

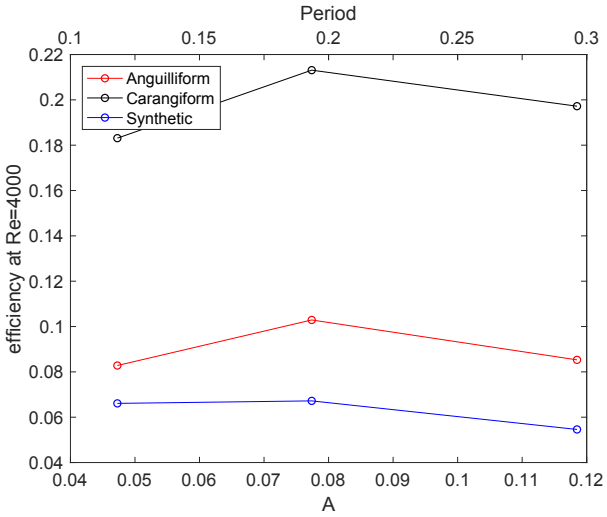

fig. 6.4 η at Re=4000

The plots in *Fig. 6.1, Fig. 6.2, and Fig. 6.3* show that it is not possible to find a general trend of the efficiency. As regards the carangiform kinematic, at Re=1000 the efficiency increases as the amplitude and the period decreases, however, at Re=4000, the efficiency has a maximum corresponding to the middle amplitude value. This trend can also be observed for the anguilliform style at both Re_0, although we recognize that the efficiency values are close to each other for the different amplitude values. As concerns the synthetic kinematic, we observe a maximum for the middle amplitude value at Re=4000, however, the efficiency increases with the amplitude for the tests at Re=1000. Generally, the efficiency values are higher for higher Re_0, except for the carangiform and synthetic kinematic for the highest amplitude value. The plots in *Fig. 6.4 and Fig. 6.5* show that for the same value of Re_0, the carangiform kinematic seems to be the most efficient, while the synthetic style has the worst performance.

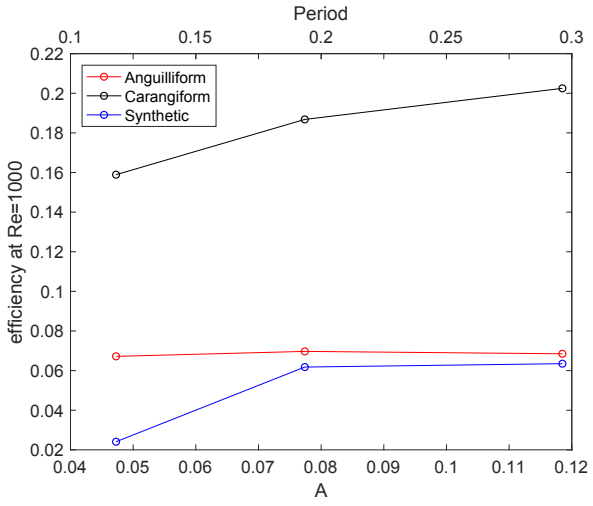

fig. 6.5 η at Re=1000

Compared to the results obtained in *Chapter 5* for the efficiency η_{EBT} calculated with the EBT model, the values listed in *Tab. 6.1, 6.2, 6.3, 6.4, 6.5 and 6.6* are definitely lower (*Tab. 6.10*). The trend observed for η_{EBT} is the same as the one observed for η only for the carangiform and the synthetic kinematic at Re=1000. Moreover, η_{EBT} and η are not agreeing on which kinematic has the best performance at equal Re_0 number.

This discrepancy was noticed in previous studies too [4], and it could be due either to the fact that the EBT model does not give a fulfilling approximation for the efficiency in our case, or to the difficulty in defining the expended power to apply to expression *6.1.*

Kinematic	Re_0	Mean η_{EBT} value	Mean η value
Carangiform	4000	0.7487	0.1978
Carangiform	1000	0.6939	0.1827
Anguilliform	4000	0.811	0.0903
Anguilliform	1000	0.7427	0.0684
Synthetic	4000	0.7698	0.0626
Synthetic	1000	0.7201	0.0498

Table 6.10: Mean η_{EBT} values and mean η values for each of the kinematics and the simulated Re_0 numbers

Chapter 7

Wake observation

The wake behind a swimming fish bears a lot of information regarding its gait, therefore it has attracted the attention of many researchers. Thanks to our model we are able to observe the wake of our simulated fish and compare it to the results of previous studies.
Figure *7.1* shows the vortex street of a carangiform fish. This is clearly an example of inverted Karman vortex street, because it consists of two rows of single counter-rotating vortices that point downstream, resembling a lot the example shown in *Fig. 2.4*. As explained in *Chapter 2*, carangiform swimmers can only produce single vortex wakes, and these can either be a standard Karman vortex street or a reverse Karman vortex street, the first being of drag type and the second being of thrust type. In the tests we performed, only inverted Karman vortex street were seen. The wake behind an anguilliform fish, can be a single vortex street like the one

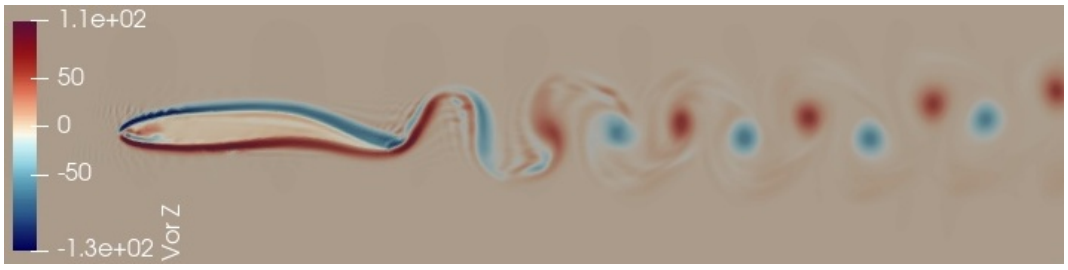

fig. 7.1 Carangiform kinematic, amplitude 0.07739, Re_0=4000

showed in *Fig. 7.2*, which is similar to the wake of a carangiform swimmer, or a double vortex street. The latter consists of two rows of double counter-rotating vortices, as shown in *Fig. 7.3*. This happens with elongated bodies because the vortex created by the undulation of the body and the one generated by the tail beating do not merge when shed. According to Borazjani the single wake happens at low St numbers, while the double wake happens at high St numbers, and the St at which the transition from single to double occurs, depends on the Reynolds

number. An example of double vortex wake (*Fig. 7.3*) was in fact observed in our simulation at St=0.2552 for the maximum amplitude at Re_0=4000, but at Re_0=1000 only single wakes were observed, even though the St numbers are higher than the ones at Re_0=4000.

As concerns the synthetic kinematic, the wake is similar to the carangiform wake, however we should not forget that no real fish swims with the synthetic deformation.

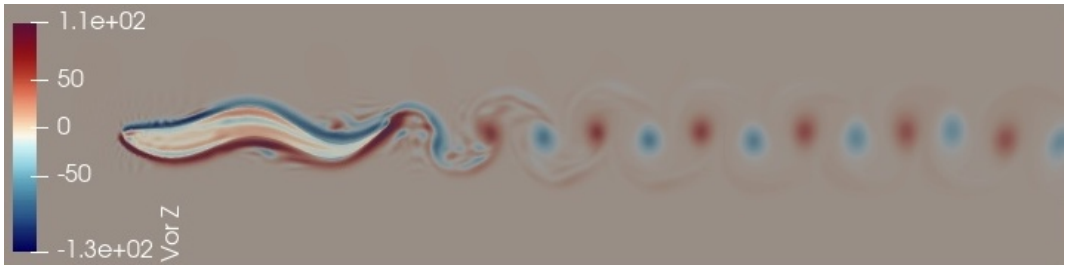

fig. 7.2 Anguilliform kinematic, amplitude 0.07739, Re_0=4000

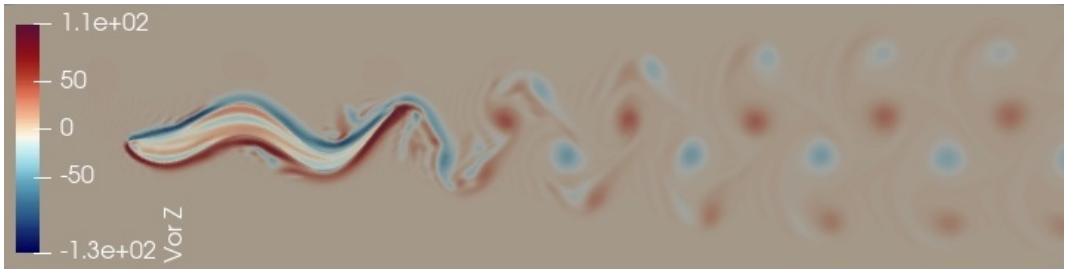

fig. 7.3 Anguilliform kinematic, amplitude 0.1185, Re_0=4000

Chapter 8

Conclusion

The study of fish locomotion has attracted the attention of many scientists throughout the centuries and it has become an important subject nowadays with the increasing attention for the environmental issues. Thanks to recent developments in computational fluid dynamics, we were able to perform 2D numerical simulations of fish swimming and to study the role of some important parameters of fish motion.

This study focused on the role of the deformation amplitude and the consequent variation of the tail beating frequency. As stated in previous studies, we found out that fish swimming with a certain tail beat frequency are able to reach a higher velocity if they increase their deformation amplitude, however things become different once both the amplitude and the frequency vary. In this case in fact, the mean velocity reached by the fish increases as the the amplitude decreases and the frequency increases, which means that if a fish is interested in being fast, it should prefer a smaller amplitude deformation and a higher frequency. This velocity trend was observed with all of the three kinematics that were tested and at both the tested values of Re_0, however the simulations have shown that the synthetic kinematic is the fastest, and the anguilliform is the slowest.

We also attempt an efficiency evaluation: first of all through the Elongated Body Theory, then with a classical definition of efficiency.

The results obtained with the model showed that the efficiency increases as the amplitude increases and the frequency decreases and that a higher Re_0 means a higher efficiency value. This means that swimming with a high velocity implies a worse performance. The results also highlighted the fact that the anguilliform kinematic is the most efficient, while the carangiform one has the lowest efficiency values.

Using the classical definition of efficiency, however, we obtained different results. In many cases

there seems to be a maximum value of efficiency for the middle value of the amplitude, and the carangiform kinematic resulted in being the most efficient, while the synthetic one has the worst performance.

The matter of efficiency and performance evaluation is however complicated and the different results we obtained are either due to the fact that the EBT model is not suited to our case, or the fact that the classical definition of efficiency is not simple to apply in the case of a self-propelled body, because of the difficulty in defining the expended power.

Finally, the wake behind a carangiform and an anguilliform fish were analysed, finding similarities with the results of previous studies.

In conclusion, we feel that the results obtained are fulfilling, but further research could clarify the definition of the required power and find a better expression for the efficiency. We also believe that a 3D model could offer a more realistic simulation, allowing to explore more aspects of fish locomotion, for instance the role of fins and appendages, and to this purpose, our study represents a starting point for any of this future developments.

Bibliography

[1] D. Paniccia, G. Graziani, C. Lugni, R. Piva "*On the role of added mass and vorticity release for self-propelled aquatic locomotion*" J. Fluid Mech. (2021)

[2] J. Gray "*The relationship between waves of muscular contraction and the propulsive mechanism of the eel*" Laboratory of Experimental Zoology, Cambridge (1933)

[3] J. Gray "*The movement of fish with special reference to the eel*" Laboratory of Experimental Zoology, Cambridge (1933)

[4] I. Borazjani, F. Sotiropoulos "*Numerical investigation of the hydrodynamics of anguilliform swimming in the transitional and inertial flow regimes*" The Journal of Experimental Biology (2008)

[5] Jun Zhang "*Footprints of a flapping wing*" J. Fluid Mech. (2017)

[6] U.K. Muller, B.L.E. Van Den Heuvel, E.J. Stamhuis, J.J Videler "*Fish foot prints: morphology and energetics of the wake behind a continuously swimming mullet*" The Journal of Experimental Biology (1997)

[7] A. Andersen, T. Bohr, T. Schnipper, J.H. Walther "*Wake structure and thrust generation of a flapping foil in two-dimensional flow*" J. Fluid Mech. (2017)

[8] U.K. Muller, J. Smit, E.J. Stamhuis, J.J.Videler "*How the body contributes to the wake in undulatory fish swimming: flow fields of a swimming eel*" The Journal of Experimental Biology (2001)

[9] A.P. Maertens, M.S. Triantafyllou, D.K.P. Yue "*Efficiency of fish propulsion*" Bioinspiration and Biomimetics (2015)

[10] W.W. Schultz, P.W. Webb "*Power requirements of swimming: do new methods resolve old questions?*" Integrative and Comparative Biology (2002)

[11] I. Borazjani "*Numerical simulations of fluid-structure interaction problems in biological flows*" PhD thesis, University of Minnesota (2008)

[12] R. Mittal G. Iaccarino "*Immersed boundary methods*" Annual Review Fluid Mechanic (2005)

[13] Z. Cui Z. Yang H. Jiang "*Sharp interface immersed boundary method for simulating three-dimensional swimming fish*" Engineering Applications of Computational Fluid Mechanics (2020)

[14] I. Borazjani F. sotiropoulos "*On the role of form and kinematics on the hydrodynamics of self-propelled body/caudal fin swimming*" The Journal of Experimental Biology (2009)